Available online at www.sciencedirect.com
ScienceDirect
Journal of Solid State Chemistry 179 (2006) 3151–3158
JOURNAL OF SOLID STATE CHEMISTRY
www.elsevier.com/locate/jssc

Formation of $LiAl_yNi_{1-y}O_2$ solid solutions under high and atmospheric pressure

E. Shinova, E. Zhecheva*, R. Stoyanova

Institute of General and Inorganic Chemistry, Bulgarian Academy of Sciences, 1113 Sofia, Bulgaria

Received 15 March 2006; received in revised form 7 June 2006; accepted 10 June 2006
Available online 16 June 2006

Abstract

Three methods were used for the synthesis of $LiAl_yNi_{1-y}O_2$ solid solutions with layered crystal structure: citrate and hydroxide precursor methods at atmospheric pressure and high-pressure synthesis in oxygen-rich atmosphere (3 GPa). Structural characterization of the oxides was performed by powder XRD analysis and electron paramagnetic resonance (EPR) spectroscopy. Irrespective of the different preparation techniques used, it was found that $LiAl_yNi_{1-y}O_2$ solid solutions can be formed in the limited concentration range of $0 \leqslant y \leqslant 0.5$ and $0.75 \leqslant y \leqslant 1.0$. The unit cell parameter a decreases linearly with the Al content whereas the unit cell parameter c increases sharper as compared to the linear interpolation of the c parameter calculated for the two end compositions $LiNiO_2$ and $LiAlO_2$. In these compositions, aluminum substitutes for Ni in the NiO_2-layer, the mean Al_yNi_{1-y}–O bond length decreasing. The extent of the trigonal distortion of $Al_yNi_{1-y}O_6$ and LiO_6-octahedra varies with the aluminum content and depends on the synthesis procedure used. The LiO_6-octahedra are more flexible to tolerate the increased trigonal distortion as compared to the $Al_yNi_{1-y}O_6$-octahedra. High-pressure synthesis favors the formation of oxides with a higher extent of trigonal distortion of both $Al_yNi_{1-y}O_6$ and LiO_6-octahedra. From EPR measurements, it was shown that local cationic distribution in $LiAl_yNi_{1-y}O_2$ depends on the synthesis temperature. At atmospheric pressure, higher synthesis temperatures promote the reaction of cation mixing between the layers.

Keywords: High-pressure synthesis; Lithium transition metal oxides; Cationic distribution; Cathode minerals for lithium ion batteries

1. Introduction

Isovalent substitution of electrochemically inactive ions for nickel ions has been reported to affect the electrochemical properties of lithium nickelates used as cathode materials for lithium ion batteries [1,2]. Among electrochemically inactive ions, Al has been preferred due to lower cost and environmental benignity [3–12]. In addition, it has been found that Al substitution leads to an increase in the electrode potential where the reversible Li intercalation takes place [14,15]. Al-substituted oxides have been reported to display better thermal stability in delithiated state as compared to pure $LiNiO_2$ [8–13].

The crystal structure of $LiNiO_2$ is composed of LiO_2- and NiO_2-layers comprising edge sharing LiO_6 and NiO_6 octahedra [16]. Due to the thermal instability of Ni^{3+}, non-stoichiometric lithium nickelates, $Li_{1-x}Ni_{1+x}O_2$ are usually obtained, where part of the Ni^{2+} ions occupy the Li-sites [17,18]. It has been found that the synthesis conditions have a strong effect on the composition and crystal structure of lithium nickelates [17,18]. To obtain nearly stoichiometric oxides, the temperature of 700 °C and oxygen atmosphere are needed. $LiAlO_2$ possesses three structural modifications [19,20]: α-$LiAlO_2$ is isostructural to layered $LiNiO_2$ and is converted, during heating above 600 °C, into γ-$LiAlO_2$, where Li and Al occupy tetrahedral sites only. The layered modification of of $LiAlO_2$ (α-form) has been obtained at intermediate pressure (3.5 GPa) [19,20] or by solid-state reaction at atmospheric pressure and 600 °C between boehmite AlOOH and Li_2CO_3 [22]. At pressure above 9 GPa, a third structural modification of $LiAlO_2$ with tetragonal structure and octahedral coordination of Al and Li has been isolated [21].

Contrary to $LiNiO_2$, Al ions in the LiO_2-layers have not been detected in α-$LiAlO_2$ irrespective of the synthesis

*Corresponding author. Fax: +359 2 870 50 24.
E-mail address: zhecheva@svr.igic.bas.bg (E. Zhecheva).

0022-4596/$ - see front matter © 2006 Elsevier Inc. All rights reserved.
doi:10.1016/j.jssc.2006.06.011

method. Layered $LiAlO_2$ and $LiNiO_2$ have been shown to react, forming $LiAl_yNi_{1-y}O_2$ solid solutions in the limited concentration range $0 \leqslant y \leqslant 0.5$, where Al substitutes for Ni in $Al_yNi_{1-y}O_2$-layers [3–12]. To our knowledge, no data on the formation of Al-rich compositions are reported in the literature. In addition, the energy calculations of the phase diagram of $LiNiO_2$–$LiAlO_2$ show miscibility gaps at low temperature, but $LiNiO_2$ forms solid solutions with $LiAlO_2$ at room temperature [23]. To understand the electrochemical behavior of substituted oxides in an extended concentration range, there is a need for detailed knowledge of their crystal chemistry.

The aim of this paper is a detailed study on the formation of $LiAl_yNi_{1-y}O_2$ solid solutions in the whole concentration range. For the preparation of $LiAl_yNi_{1-y}O_2$ we have applied synthesis methods under atmospheric and high pressures. At atmospheric pressure, the citrate and hydroxide precursor methods were used. High-pressure syntheses (3 GPa) were performed in oxygen-rich atmosphere using one piston cylinder apparatus with the intention to stabilize both Al^{3+} and Ni^{3+} ions in octahedral coordination. Powder XRD analysis was used for structural characterization of $LiAl_yNi_{1-y}O_2$. The oxidation state of Ni ions and the local cationic distribution in $LiAl_yNi_{1-y}O_2$ were analyzed by electron paramagnetic resonance (EPR) spectroscopy.

2. Experimental

$LiNi_{1-y}Al_yO_2$ solid solutions were prepared by the citrate precursor method. Lithium–nickel–aluminum citric acid compositions were obtained by dissolution of $LiOH \cdot H_2O$, $Ni(OH)_2$, and $Al(NO_3)_3 \cdot 9H_2O$ in aqueous solutions of citric acid (0.1 M). The ratio between the components was Li:(Ni + Al):Cit = 1.05:1:1. Heating at 80 °C yielded a transparent solution which was concentrated to 0.5 M Li. After complexation, the solution obtained was cooled down to room temperature, then frozen instantly with liquid nitrogen and dried in vacuum (20–30 mbar) at −20 °C with an Alpha-Crist Freeze-Dryer. After drying, the solid residues were decomposed at 500 °C with a heating rate of 1°/min and were further heated at 700, 750 and 800 °C for 20–120 h in oxygen.

Al-rich compositions were prepared following the procedure for the preparation of layered $LiAlO_2$ at 600 °C [22]. Mixed Al and Ni hydroxides were synthesized by co-precipitation of $Ni(NO_3)_2 \cdot 6H_2O$ and $Al(NO_3)_3 \cdot 9H_2O$ by ammonia. The solid residue was dried under vacuum at 100 °C. The co-precipitated Al and Ni hydroxides were mixed thoroughly with Li_2CO_3. The mixture obtained was heated at 600 °C for 25 h in air.

For the preparation of $LiAl_yNi_{1-y}O_2$ under high pressure we adopted the synthesis procedure described in [24] for the preparation of layered $LiAlO_2$. The mixture of Li_2O_2 with NiO (obtained by thermal decomposition of nickel hydroxide at 550 °C) and Al_2O_3 was sealed in an Au or a Pt-capsule. The solid-state reaction proceeded at 700 °C for 5 h in one piston cylinder type apparatus. When the reaction took place in a Pt-capsule, an unusual splitting of the (003) diffraction line of the layered structure was observed for Al-rich compositions only. In the case of pure $LiAlO_2$ Chang and Margrave [24] have explained the splitting of this diffraction line by the formation under the high-pressure of the fourth modification of $LiAlO_2$ with monoclinic structure. For the samples prepared by us, the EDAX and XRD analysis shows clearly that this splitting is due to the appearance of Li_2PtO_3 as an impurity phase in Al-rich compositions prepared in the Pt-capsule. To avoid the formation of the impurity Li_2PtO_3 phase, the reaction mixture of Li_2O_2 with NiO–Al_2O_3 was sealed in an Au-capsule.

High-pressure synthesis was carried out in a 1/2 inch end-loaded piston-cylinder apparatus at the Bayerisches Geoinstitut. Experiments were performed using the "hot-piston in" technique. Samples were encapsulated in 1 cm long, 5 mm diameter welded Au capsules. Details of the high-pressure experiments are given elsewhere [25,26].

The lithium content of the samples, the mean oxidation state of nickel and the total nickel and aluminum content were determined by atomic absorption analysis, iodometric titration and complexometric titration, respectively.

X-ray phase analysis was carried out on a Philips X'Pert powder diffractometer with Co$K\alpha$-radiation, reflection mode, and with a Si internal standard. The scan range $15 \leqslant 2\Theta \leqslant 120$ in a step increment of 0.02° was utilized. The Fullprof computer program was used for the calculation [27]. The diffractometer point zero, Lorentzian/Gaussian fraction of the pseudo-Voigt peak function, scale factor, lattice constants (a and c), oxygen parameter (z), thermal factors for 3a, 3b and 6c positions, half-width parameters, preferred orientation were refined. To gain stability during the refinement, the Al/Ni-ratio was imposed by the chemical composition of the oxides. Subsequently, the cationic occupancy factors were refined taking into account that the total occupancies of the 3a and 3b sites were equal to unity.

EPR measurements at 9.23 GHz (X-band) were carried out in an ERS 220/Q spectrometer within the temperature range 85–410 K. The high-frequency EPR spectra were recorded at a single-pass transmission EPR spectrometer built in the High-Magnetic Filed Laboratory, Grenoble, France. The frequencies were changed from 95 to 345 GHz using Gunn diodes and their multipliers. The detection of absorption was performed with an bolometer. The recording temperatures were varied between 5 and 100 K using a variable temperature insert (Oxford Instruments).

3. Results

3.1. Crystal structure of $LiAl_yNi_{1-y}O_2$ solid solutions

The solubility of Al into layered $LiNiO_2$ depends on the kind of synthesis procedure used. The citrate precursor method allows preparing $LiAl_yNi_{1-y}O_2$ solid solutions

where Al content varies between 0% and 50%. Above $y>0.5$, a mixture between γ-$LiAlO_2$ and an Al-poor composition ($y \approx 0.5$) is obtained when the citrate precursor method is used. Aluminum-rich compositions with $0.75 \leqslant y \leqslant 1.0$ are successfully prepared under atmospheric pressure using the hydroxide precursors. High-pressure synthesis yields two type of compositions: $LiAl_yNi_{1-y}O_2$ with $0 \leqslant y < 0.5$ and $LiAl_yNi_{1-y}O_2$ with $0.8 < y \leqslant 1.0$ (Fig. 1). Any attempts to prepare the intermediate compositions with $0.5 < y < 0.75$ were unsuccessful (Fig. 1). High-pressure synthesis of $LiAl_yNi_{1-y}O_2$ with $0.5 < y < 0.75$ led to the phase separation into Al-poor and Al-rich compositions ($y < 0.1$ and > 0.85, Fig. 1), while mixtures of γ-$LiAlO_2$ and Al-poor compositions ($y \approx 0.5$) were obtained for this composition range under atmospheric pressure.

The XRD patterns of all the samples obtained are indexed in the *R*-3*m* space group: Li and Ni occupy 3*b* and 3*a* positions and O is in the 6*c* position (Fig. 1). As in the case of pure lithium nickelates, an improved fitting of the XRD patterns was achieved when a small fraction of Ni resides on the Li-site. The oxides prepared under atmospheric pressure display a higher amount of Ni in the Li-site as compared to oxides prepared under a high-pressure (Table 1). The amount of Ni in the Li-site is sensitive towards the Al-to-Ni ratio. Al-poor oxides display a higher

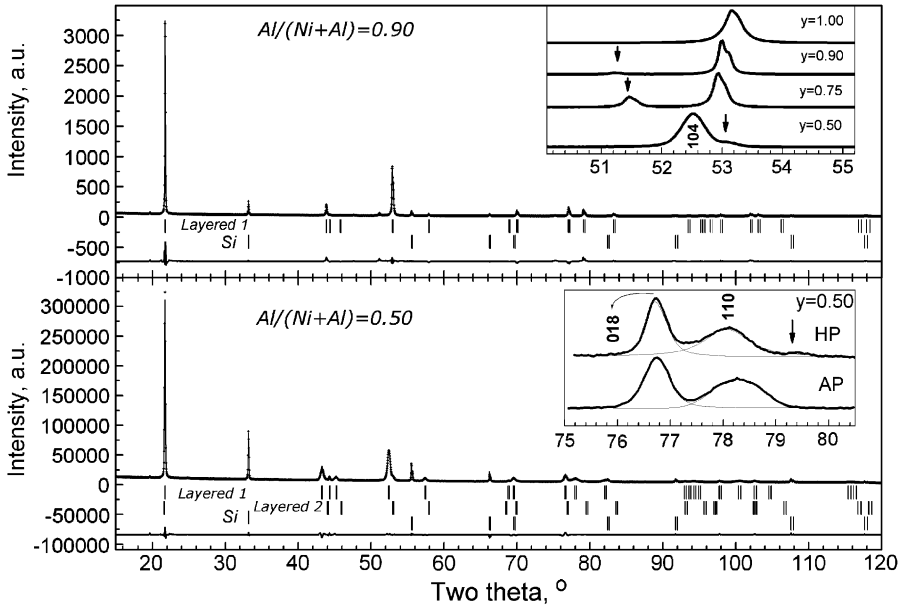

Fig. 1. XRD patterns and fitting by Rietveld procedure of $LiAl_yNi_{1-y}O_2$ synthesized at high oxygen pressure and 700 °C. The difference between the observed and calculated profiles is plotted. Bragg reflections for layered $LiAl_yNi_{1-y}O_2$ and Si standard are indicated. The arrow indicates the second phase with layered structure. Selective broadening of the (1 1 0) diffraction line as compared to (018) diffraction line is shown for $LiNi_{0.5}Al_{0.5}O_2$ obtained under high pressure and from citrate precursors.

Table 1
Structural parameters (unit cell parameters *a* and *c*, and nickel occupancy in the lithium layers, δ) determined from Rietveld refinement of the XRD patterns and the slope of the temperature dependence of the EPR line width dH_{pp}/dT for $Li_{1-\delta}Ni_\delta[Al_yNi_{1-y}]O_2$ oxides obtained from citrate (citrate) and hydroxide precursors (OH) at atmospheric pressure and under high pressure in an oxygen atmosphere (H-P)

Y	Method of preparation	*a* (Å)	*c* (Å)	δ ($\pm$0.004)	dH_{pp}/dT (mT/K)
0.0	H-P	2.8769	14.1827	0.014	0.421
0.05	H-P	2.8742	14.1880	0.006	0.368
0.10	H-P	2.8720	14.2007	0.009	0.360
0.42	H-P	2.8454	14.2516	0.0	—
0.90	H-P	2.8084	14.2344	0.0	—
1.0	H-P	2.8009	14.2253	0.0	—
0.0	Citrate	2.8772	14.1883	0.054	0.37
0.12	Citrate	2.8685	14.1997	0.035	0.18
0.50	Citrate	2.8372	14.2535	0.009	—
0.76	OH	2.8158	14.2620	0.014	—
0.94	OH	2.8082	14.2332	0.011	—
1.0	OH	2.8053	14.2108	0.0	—

Ni content in the LiO_2-layers, while Al-rich oxides obtained under a high pressure are characterized by Ni-free LiO_2-layers (Table 1). It is worth mentioning that $LiAl_yNi_{1-y}O_2$ oxides with Ni amount in the Li-site less than 4% were obtained in the whole Al concentration range. Another feature of the XRD patterns of Al-poor oxides is the selective broadening of the (110) diffraction line as compared to that of the (108) diffraction line, especially in the case of $LiAl_yNi_{1-y}O_2$ with $y = 0.50$ (Figs. 1 and 2). The selective broadening is observed with both types of oxides prepared under high- and atmospheric pressure (Fig. 1). This has already been reported for $LiAl_yNi_{1-y}O_2$ prepared under atmospheric pressure and has been explained by short-range inhomogeneity, such as a tendency to aluminum clustering [3,9]. In addition, at atmospheric pressure, the selective broadening of the (110) diffraction line slightly decreased when the oxides are prepared at higher temperatures (Fig. 2). This observation means that the preparation temperatures influence the short-range Al inhomogeneity. It is worth mentioning that short-range Al inhomogeneity does not appear for Al-rich compositions with $y \geqslant 0.75$ (Fig. 2).

The effect of the Al content on the unit cell dimensions of $LiAl_yNi_{1-y}O_2$ is shown on Fig. 3. The unit cell parameter a decreases linearly with the Al substitution. It is noticeable that the unit cell dimensions for solid solutions with layered crystal structures have usually been found to display the Vegard's like behavior, with the exception of compositions with a partial occupancy of metal ions in the LiO_2-layers [28–31]. In this context, the a-parameter was shown in Fig. 3 for oxides with the minimum amount of Ni ions in the Li-site (less than 4%). In addition, it is important that the synthesis method does not affect the unit cell parameter a. In contrast, the unit cell parameter c increases sharper with the Al content compared to a linear interpolation of the c parameter calculated from the two end members $LiNiO_2$ and $LiAlO_2$. For Al-rich oxides, the unit cell parameter c is different with oxides prepared under atmospheric or high pressures. The observed variation in the unit cell parameters a and c reveals the structural anisotropy of the layered structure.

For the trigonal structure, the a-parameter gives the distance between the metal ions in the layers and can be

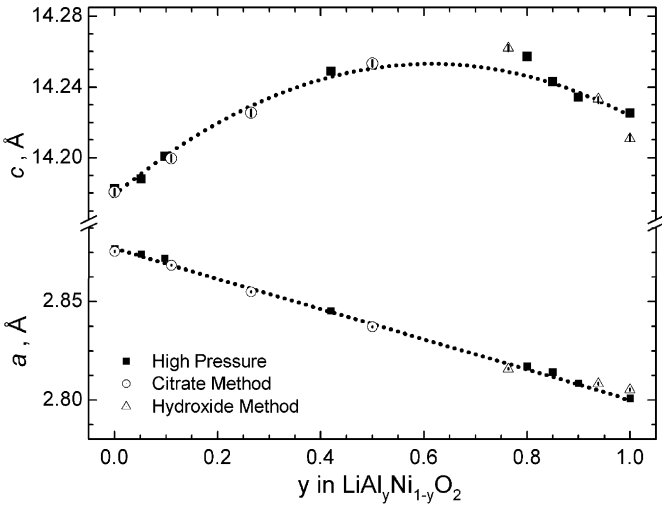

Fig. 3. Unit cell parameters (a and c) vs. Al content for $LiAl_yNi_{1-y}O_2$ solid solutions synthesized under high oxygen pressure, as well as at atmospheric pressure from citrate and hydroxide precursors.

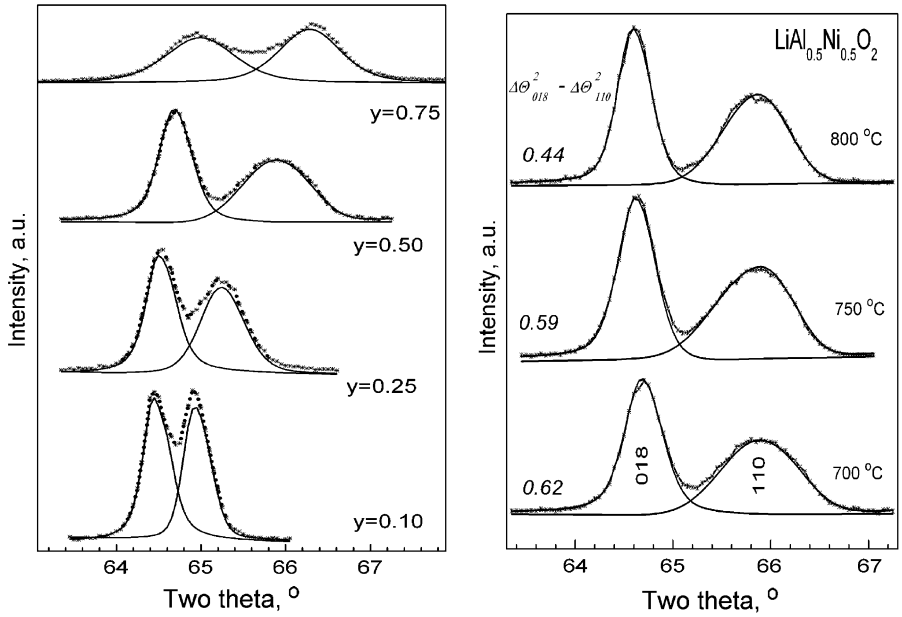

Fig. 2. The (018) and (110) diffraction lines for $LiAl_yNi_{1-y}O_2$ prepared at atmospheric pressure (left): $y = 0.10, 0.25, 0.50$ prepared at 700 °C from citrate precursor and $y = 0.75$ prepared at 600 °C from hydroxide precursor. The effect of the synthesis temperature on the (018) and (110) diffraction lines for $LiAl_{0.5}Ni_{0.5}O_2$ is shown (right). The difference in the line width of (018) and (110) diffraction lines for $LiAl_{0.5}Ni_{0.5}O_2$ is also shown ($\Delta\Theta^2_{018} - \Delta\Theta^2_{110}$, right).

expressed by

$$a = 2^{1/2} r_{M-O}(1 - \cos\alpha_{M-O-M})^{1/2}$$
$$= 2^{1/2} r_{Li-O}(1 - \cos\alpha_{Li-O-Li})^{1/2},$$

where r_{M-O} and r_{Li-O} denote the mean Al_yNi_{1-y}–O and Li–O bond lengths, α_{M-O-M} and $\alpha_{Li-O-Li}$ are the angles between two neighboring ions via oxygen. The structural anisotropy of the layered structure can be expressed by the thickness of the $Al_yNi_{1-y}O_2$ and LiO_2-layers, $S_{Al_yNi_{(1-y)}O_2}$ and S_{LiO_2} (i.e. the distance separating two opposite faces of the octahedra along [001]), which are related to the c-parameter as follows:

$$c = S_{Al_yNi_{(1-y)}O_2}/(2/3 - 2z)) = S_{LiO_2}/(2z - 1/3),$$

where z is the oxygen parameter. Furthermore, the extent of the trigonal distortion of the $Al_yNi_{1-y}O_6$ and the LiO_6 octahedra in the $Al_yNi_{1-y}O_2$ and LiO_2-layers can be evaluated by the ratio between the layer thickness, $S_{Al_yNi_{(1-y)}O_2}$ and S_{LiO_2}, and the unit cell parameter a. For undistorted octahedron this value is 0.816.

Fig. 4 gives the variation in the mean $Ni_{1-y}Al_y$–O and Li–O bond lengths. The mean $Ni_{1-y}Al_y$–O bond length decreases with an increase in the Al-content. This trend is consistent with the lower ionic radius of Al^{3+} as compared to Ni^{3+} ions. In the same sequence the mean Li–O bond length decreases slightly (Fig. 4). In addition, the mean $Ni_{1-y}Al_y$–O and Li–O bond lengths are sensitive towards the synthesis procedure used. When oxides are prepared under a high pressure, the mean $Ni_{1-y}Al_y$–O bond length decreases more rapidly as compared with the mean value of Ni–O and Al–O bond lengths determined for two end compositions $LiNiO_2$ and $LiAlO_2$. In comparison with

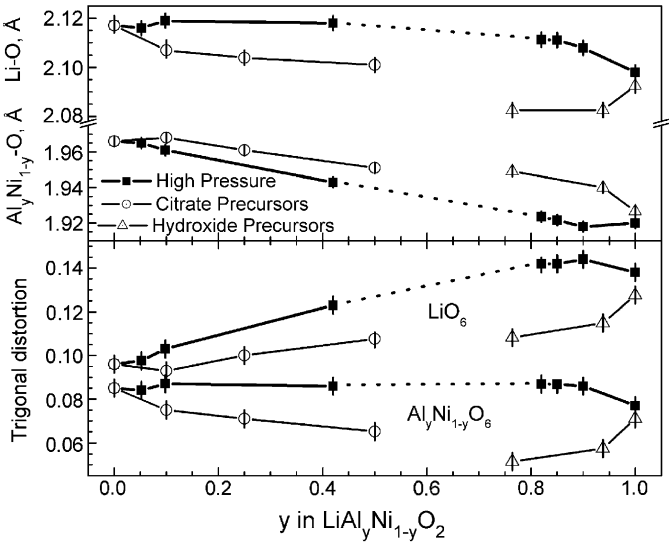

Fig. 4. The mean Al_yNi_{1-y}–O and Li–O bond lengths (upper) and the deviation of the experimentally determined extent of the trigonal distortion of $Al_yNi_{1-y}O_6$- and LiO_6-octahedra from that of undistorted octahedron as a function of the Al-content for $LiAl_yNi_{1-y}O_2$ solid solutions synthesized under high oxygen pressure, as well as at atmospheric pressure from citrate and hydroxide precursors.

$Ni_{1-y}Al_y$–O, the mean Li–O bond length is more sensitive towards the synthesis procedure used. This fact can be related to the strength of the trigonal distortion of the unit cell.

Fig. 4 also gives the deviation of the experimentally determined extent of the trigonal distortion from that of undistorted octahedron as a function of the Al-content: ($|S_{Al_yNi_{(1-y)}O_2}/a - 0.816|$ and $|S_{LiO_2}/a - 0.816|$). It is clear that high-pressure synthesis favors the formation of oxides characterized by a higher extent of trigonal distortion of both $Al_yNi_{1-y}O_6$ and LiO_6-octaheda. It is noticeable that the LiO_6-octahedra are more flexible to tolerate the increased trigonal distortion as compared to the $Al_yNi_{1-y}O_6$-octahedra. The increased trigonal distortion of the LiO_6-octahedra together with the increased thickness of the LiO_2-layers would have a positive effect on Li diffusion. This feature would be favorable for the electrochemical properties of $LiAl_yNi_{1-y}O_2$ when used as cathode materials in lithium ion batteries. However, using molecular dynamics simulations, it has been demonstrated that the extension of the LiO_2-layer leads to destabilization of the trigonal structure [32]. Moreover, according to Buta et al. [23] the large difference in the ionic dimensions of transition metal ions and Al^{3+} causes strains in the crystal structure, resulting in a greater tendency for phase separation. This agrees well with the observed lack of $LiAl_yNi_{1-y}O_2$ solid solutions in the range $0.5 < y < 0.75$.

3.2. EPR spectroscopy of $LiAl_yNi_{1-y}O_2$ solid solutions

Nearly stoichiometric $LiNiO_2$ has been shown to exhibit an EPR spectrum consisting of a single Lorentzian line with $g = 2.137$ due to low spin Ni^{3+} ions [34]. The line shape and line width depend on the registration temperature, Jahn–Teller effect and ferromagnetic interactions between Ni^{3+} ions in the layers [35]. In the EPR spectra of Al-substituted oxides studied by us, a single Lorentzian line is still visible with the exception of $LiAlO_2$ doped with 1% Ni prepared by the hydroxide precursor methods. The substitution of Al for Ni affects both the g-factor and the line width. The g-factor decreases after replacement of Ni by Al, indicating an increased covalency of the Ni–O bond. The same effect has been found for Al-substituted lithium nickelates with $0 \leqslant y \leqslant 0.25$, as well as for layered $(1-a)LiNi_{1-y}Al_yO_2 \cdot aLi[Li_{1/3}Ni_{2/3}]O_2$ oxides obtained under high-pressure [6,26]. Fig. 5 shows the variation of the EPR line width (determined at 103 K) with Al substitution. The EPR line width increases with the Al-content, reaching a maximum at $0.25 < y < 0.5$, and decreases for Al-rich oxides. The observed changes in the EPR line width can be related to magnetic dilution of Ni^{3+}-spin systems caused by Al^{3+} ions. The replacement of paramagnetic Ni^{3+} by diamagnetic Al^{3+} ions will suppress the development of exchange interactions between Ni^{3+} ions leading to the increase in the EPR line width. In the same sequence, the dipole–dipole interactions between Ni^{3+} ions will be diminished resulting in a signal

narrowing. The competition between exchange and dipole–dipole interactions determines the dependence of the EPR line width on the Al-to-Ni ratio (Fig. 5).

The temperature variation of the EPR line width, ΔH_{pp}, is also affected by the Al substitution (Fig. 6). For oxides with $0 \leqslant y \leqslant 0.25$, there is a linear decrease in the EPR line width on cooling, while for oxides with $y \geqslant 0.5$ the EPR line width slightly depends on the registration temperature. For pure $LiNiO_2$, the $d\Delta H_{pp}/dT$ slope has been shown to depend on the strength of the 180°- and 90°-$Ni^{3+/2+}$–O–$Ni^{3+/2+}$ exchange interactions, the metal coordination number of the exchange-coupled particles and on the distance between them [34,35]. The slope of the linear dependence, $d\Delta H_{pp}/dT$, decreases with the reduction of the amount of Ni^{2+} in the lithium layers [35]. Further decrease in $d\Delta H_{pp}/dT$ is observed when Al substitutes for Ni, $Li_{1-\delta}Ni_{\delta}[Al_yNi_{1-y}]O_2$ (Fig. 6). This result also demonstrates the formation of solid solutions between $LiAlO_2$ and $LiNiO_2$.

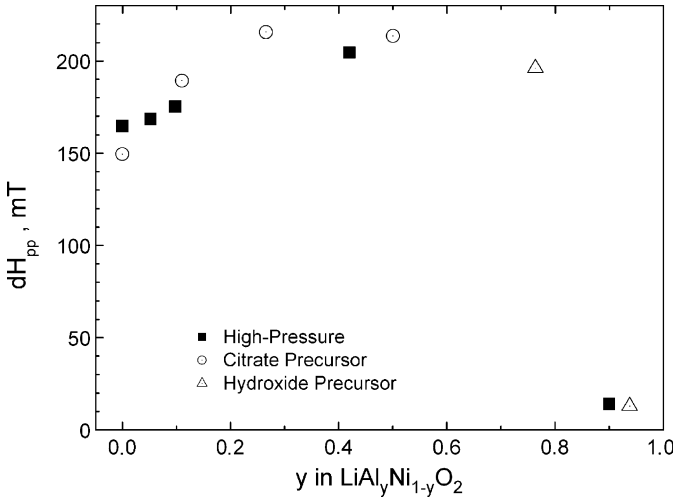

Fig. 5. EPR line width, ΔH_{pp} vs. Al content for $LiAl_yNi_{1-y}O_2$ solid solutions synthesized under high oxygen pressure, as well as at atmospheric pressure from citrate and hydroxide precursors.

In addition, for pure $LiNiO_2$ the value of $d\Delta H_{pp}/dT$ has been found to depend on the preparation temperature of pure $LiNiO_2$ [33]: the extrapolated values for samples obtained at 700 and 800 °C are 0.26 and 0.46 mT/K, respectively. Based on this dependence, it has been inferred that higher synthesis temperatures (800 °C) favor reactions of intrinsic disorder, i.e. the cationic mixing between the LiO_2- and NiO_2-layers [33]. Owing to the small scattering factor for Li, the XRD method does not permit detection of this type of reactions. In comparison with $LiNiO_2$ oxides prepared at atmospheric pressure, oxides prepared under a high pressure display a higher value of the $d\Delta H_{pp}/dT$ slope: 0.492 and 0.421 mT/K for $Li_{1-\delta}Ni_{1+\delta}O_2$ with $\delta = 0.055$ and 0.014, respectively [25]. This observation is in agreement with the effect of high-pressure synthesis on the cationic distribution in $LiNiO_2$. It has been found that the high pressure facilitates the insertion of Li into NiO_2-layers, $Li[Li_xNi_{1-x}]O_2$ compositions being formed [25]. At atmospheric pressure, the formation of $Li[Li_{1/3}Ni_{2/3}]O_2$ has not been reported. Returning to our samples, this dependence of $d\Delta H_{pp}/dT$ on the synthesis temperature was also obeyed for oxides containing 10% Al. The $[Li_{1-\delta}Ni_{\delta}][Al_{0.1}Ni_{0.9}]O_2$ oxides prepared at 700 °C display a lower value of $d\Delta H_{pp}/dT$ as compared to that for oxides prepared at 800 °C, while the value of $d\Delta H_{pp}/dT$ for oxides prepared at 750 °C falls in the intermediate range: $d\Delta H_{pp}/dT$ is 0.18, 0.21 and 0.34 mT/K for samples obtained at 700, 750 and 800 °C and characterized with $\delta = 0.035$, 0.043 and 0.049, respectively. In addition, high-pressure synthesis affects also $d\Delta H_{pp}/dT$ for $[Li_{1-\delta}Ni_{\delta}][Al_{0.1}Ni_{0.9}]O_2$ (Table 1). While the high-pressure synthesis allows preparation of oxides with minimum amount of Ni^{3+} in the Li-sites (determined by the XRD analysis), the value of $d\Delta H_{pp}/dT$ is higher: 0.46 and 0.36 mT/K for samples with $\delta = 0.038$ and 0.009 and prepared under high-pressure. As in the case of pure $LiNiO_2$, this observation can be related to the favorable effect of the high pressure on the insertion of lithium ions into the $Al_yNi_{1-y}O_2$-layers.

For the oxides with $y \geqslant 0.5$, the slight dependence of the EPR line width on the registration temperature indicates

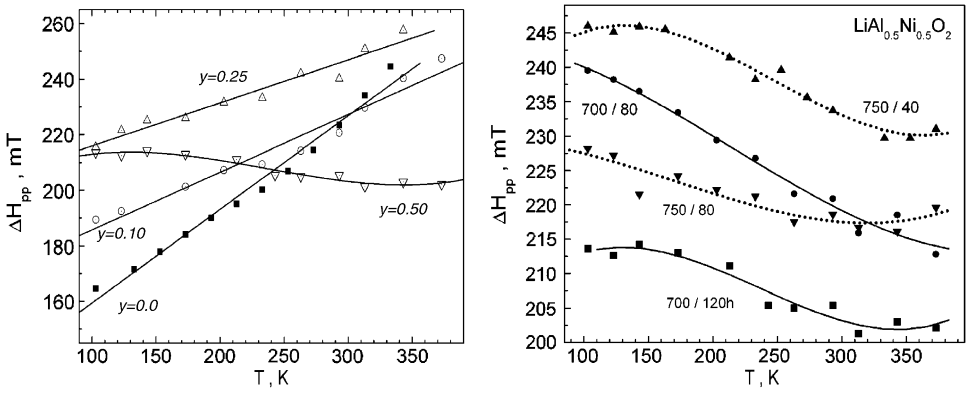

Fig. 6. Temperature variation of the EPR line width (left) for $LiAl_yNi_{1-y}O_2$ obtained from citrate precursors at 700 °C with $y = 0.0$, 0.10, 0.25 and 0.50. Temperature variation of the EPR line width (right) for $LiAl_{0.5}Ni_{0.5}O_2$ obtained from citrate precursors at 700 °C for 80 and 120 h and 750 °C for 40 and 80 h. The heating time is selected in order to compare $LiAl_{0.5}Ni_{0.5}O_2$ samples with close values of the Ni amount in the Li-site (less than 4%).

that magnetic dipole–dipole interactions dominate over the exchange interactions (Fig. 6). This is consistent with the dependence of the EPR line width on the Al-content (Fig. 5). In addition, the EPR line width for $LiAl_{0.5}Ni_{0.5}O_2$ obtained from citrate precursor is higher for oxides obtained at higher temperatures (Fig. 6). As in the case of Al-poor compositions, one can suggest that high-temperatures give rise to the reaction of cationic mixing between the layers.

For the oxide with $y = 0.75$ prepared from hydroxide precursor at 600 °C, two low-intensity signals are superimposed on the main signal (Fig. 7). The two signals have the Lorentzian line shape and a line width of 55.6 and 14.4 mT, which are much lower than that of the main EPR signal (196.1 mT). These two signals have different dependence on the registration temperature (Fig. 7). At 103 K, the intensities of both signals are much lower than that of the main signal: 1% and 4% versus 95%, respectively. The narrow signal exhibits EPR parameters

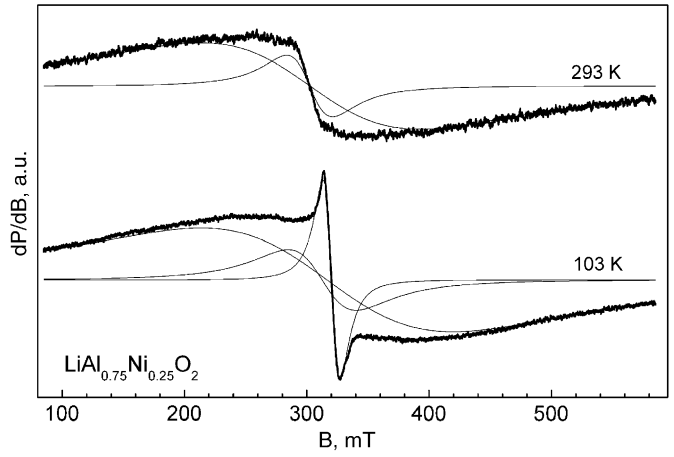

Fig. 7. The EPR spectra at 103 and 293 K of $LiAl_{0.75}Ni_{0.25}O_2$ prepared at 600 °C from hydroxide precursor.

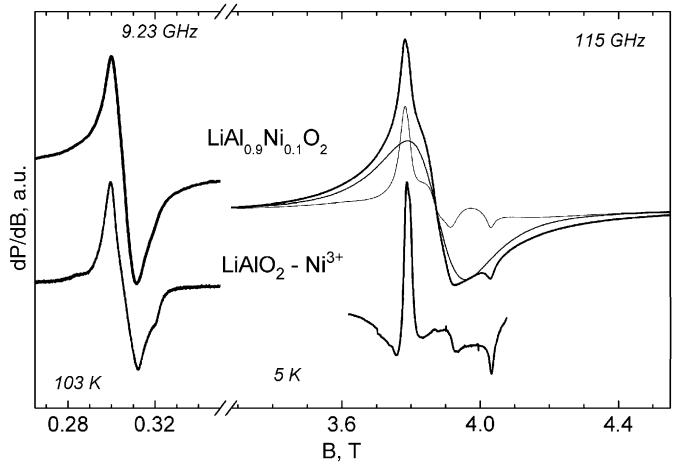

Fig. 8. X-band and high-frequency EPR spectra (9.23 and 115 GHz) of $LiAl_{0.9}Ni_{0.1}O_2$ and Ni-doped $LiAlO_2$ prepared at 600 °C from hydroxide precursor.

close to that of Ni-doped $LiAlO_2$ (see Fig. 8). According to the EPR study of Ni^{3+} in $LiNi_xCo_{1-x}O_2$ solid solutions [36], these three EPR signals can be assigned to Ni^{3+} ions having different paramagnetic/diamagnetic metal ions environments. Having in mind that in the layered structure, each metal ion has six metal neighbors in the MO_2-layers, we can assume that the main EPR signal corresponds to Ni^{3+} ions in a mixed Ni^{3+}/Al^{3+} environment with a statistical distribution, while the additional narrow signals are due to Ni^{3+} in environment of Al^{3+} mostly. For a statistical distribution of Ni and Al in the $Al_yNi_{1-y}O_2$-layers, one can expect to register only one broad EPR signal due to the convolution of the signals from different Ni^{3+} ions located in a mixed $Ni_{0.25}Al_{0.75}$-environment. The observation of two additional EPR signals in $LiAl_{0.75}Ni_{0.25}O_2$ does not contradict with the suggestion for a statistical Ni/Al distribution since their intensities are much lower as compared to that of the main signal. This means that the additional low-intensity signals come, most probably, from Ni^{3+} in defect crystal sites.

For $LiAl_{0.9}Ni_{0.1}O_2$- and Ni-doped $LiAlO_2$, the high-temperature EPR spectra exhibit a single Lotrentzian line (Fig. 8). On cooling, the symmetrical signal is transformed into a signal with tetragonal symmetry. This behavior is typical of the static Jahn–Teller effect. In order to improve the resolution of the EPR spectrum, EPR at high frequency and high magnetic field was undertaken. Fig. 8 shows the EPR spectra at 115 GHz of $LiAl_{0.9}Ni_{0.1}O_2$ and Ni-doped $LiAlO_2$. For the Ni-doped $LiAlO_2$ composition, the EPR spectrum consists of a tetragonal symmetry signal with a small anisotropy in the perpendicular region: $g_{\perp}^1 = 2.1700$, $g_{\perp}^2 = 2.1610$ and $g_{\parallel} = 2.0379$. In all cases, $g_{\perp}$ is greater than $g_{\parallel}$, indicating that the Ni^{3+} ions are in a tetragonally elongated octahedron with an $^2A_{1g}$ ground state. This observation is consistent with the EPR data on Ni^{3+} in $LiAl_yCo_{1-y}O_2$ solid solutions [37]. In the high-frequency EPR spectrum of $LiAl_{0.9}Ni_{0.1}O_2$, two overlapping signals account for the EPR profile: one signal with tetragonal symmetry and parameters close to that of Ni^{3+} in $LiAlO_2$ and second signal with symmetrical shape and $g = 2.121$. These two signals can be assigned to Ni^{3+} ions in pure Al- and in mixed Ni, Al-environment, respectively.

4. Conclusions

It was found that the incorporation of Al into the layered structure of $LiNiO_2$ is limited. At atmospheric pressure, the citrate precursor method allows preparing $LiAl_yNi_{1-y}O_2$ solid solutions in a limited concentration range: $0 \leqslant y \leqslant 0.5$. Above $y > 0.5$, a mixture between γ-$LiAlO_2$ and Al-poor composition ($y \approx 0.5$) is obtained when the citrate precursor method is used. Al-rich compositions with $y \geqslant 0.75$ are only formed under mild conditions comprising the reaction between co-precipitated Ni, Al hydroxides and $LiCO_3$ at 600 °C. Even in the case when high-pressure synthesis in oxygen-rich atmosphere is used, layered $LiAl_yNi_{1-y}O_2$ solid solutions are formed in

the limited concentration range of $0 \leqslant y \leqslant 0.5$ and $0.75 < y \leqslant 1.0$.

When Al substitutes for Ni, there is a strong contraction of the mean Al_yNi_{1-y}–O bond length concomitant with an increase of the LiO_2-layer thickness, culminating in the absence of $LiAl_yNi_{1-y}O_2$ solid solution for the $0.5 < y < 0.75$ concentration range. The extent of the trigonal distortion of both $Al_yNi_{1-y}O_6$- and LiO_6-octahedra depends on the Al content and on the preparation method used. High-pressure synthesis favors the formation of oxides with a higher extent of trigonal distortion of both $Al_yNi_{1-y}O_6$ and LiO_6-octahedra. At atmospheric pressure, higher synthesis temperature (800 °C) promotes the reaction of cationic mixing between the layers.

Acknowledgments

The authors thank the National Science Fund of Bulgaria (Contract no. Ch1304/2003) for financial support. R.S. and E.Sh. are grateful to the EC for a grant of a EU "Research Infrastructures: Transnational Access" Program (Contract no. 505320 (RITA)—High Pressure) for performing high-pressure synthesis experiments at the Bayrisches Geoinstitut, Universität Bayrewth. The high-frequency EPR measurements carried out at High Magnetic Field Laboraty in Grenoble, France, were supported by the European Commission within the Sixth framework program "Transnational Access—Specific Support Action" (Contract no. RITA-CT-2003-505474)—"Access to research in very high magnetic field". The authors are very grateful to Dr. T. Boffa-Ballaran and Dr. C. McCammon, from Bayerisches Geoinstitut, Universität Bayreuth, and Dr. A.-L. Barra, from High Magnetic Field Laboratory in Grenoble, for their help.

References

[1] M. Broussely, P. Biensan, B. Simon, Electrochim. Acta 45 (1999) 3.
[2] M.S. Whittingham, Chem. Rev. 104 (2004) 4271.
[3] T. Ohzuku, A. Ueda, M. Kouguchi, J. Electrochem. Soc. 142 (1995) 4033.
[4] O. Zhong, U. von Sacken, J. Power Sources 54 (1995) 221.
[5] T. Ohzuku, T. Yanagawa, M. Kouguchi, A. Ueda, J. Power Sources 68 (1997) 131.
[6] R. Stoyanova, E. Zhecheva, E. Kuzmanova, R. Alcántara, P. Lavela, J.L. Tirado, Solid State Ion. 128 (2000) 1.
[7] C. Julien, G.A. Nazri, A. Rougier, Solid State Ion. 135 (2000) 121.
[8] S.H. Park, K.S. Park, Y.K. Sun, K.S. Nahm, Y.S. Lee, M. Yoshio, Electrochim. Acta 46 (2001) 1215.
[9] M. Guilmard, A. Rougier, M. Grüne, L. Croguennec, C. Delmas, J. Power Sources 115 (2003) 305.
[10] J. Kim, J. Liu, C. Chen, K. Amine, J. Electrochem. Soc. 150 (2003) A1491.
[11] M.Y. Song, R. Lee, I. Kwon, Solid State Sci. 156 (2003) 319.
[12] P. Kalyani, N. Kalaiselvi, N.G. Renganathan, M. Raghavan, Mater. Res. Bull. 39 (2004) 41.
[13] M. Guilmard, L. Croguennec, C. Delmas, Chem. Mater. 15 (2003) 4484.
[14] Y.-I. Jang, B. Huang, H. Wang, G.R. Maskaly, G. Ceder, D.R. Sadoway, Y.-M. Chiang, H. Liu, H. Tamura, J. Power Sources 81 (1999) 589.
[15] T. Amriou, A. Sayede, B. Khelifa, C. Mathieu, H. Aourag, J. Power Sources 130 (2004) 213.
[16] L.D. Dyer, B.S. Borie, G.P. Smith, J. Am. Chem. Soc. 76 (1954) 1499.
[17] R. Alcántara, P. Lavela, J.-L. Tirado, E. Zhecheva, R. Stoyanova, J. Solid State Electrochem. 3 (1999) 121.
[18] C. Delmas, M. Menetrier, L. Croguennec, I. Saadoune, A. Rougier, C. Poillerie, G. Prado, M. Grüne, L. Fournes, Electrochim. Acta 145 (1999) 243.
[19] M. Marezio, J.P. Remeika, J. Chem. Phys. 44 (1966) 3143.
[20] M. Marezio, Acta Crystallogr. 19 (1965) 396.
[21] X. Li, T. Kobayashi, F. Zhang, K. Kimoto, T. Sekine, J. Solid State Chem. 177 (2004) 1939.
[22] K.R. Poeppelmeir, C.K. Chiang, D.O. Kipp, Inorg. Chem. 27 (1988) 4523.
[23] S. Buta, D. Morgan, A. Van der Ven, M.K. Aydinol, G. Ceder, J. Electrochem. Soc. 146 (1999) 4335.
[24] C.H. Chang, J.L. Margrave, J. Am. Chem. Soc. 44 (1968) 2020.
[25] E. Shinova, E. Zhecheva, R. Stoyanova, G.G. Bromiley, J. Solid State Chem. 178 (2005) 1661.
[26] E. Shinova, E. Zhecheva, R. Stoyanova, G.D. Bromiley, R. Alcántara, J.L. Tirado, J. Solid State Chem. 178 (2005) 2692.
[27] J. Rodríguez-Carvajal, in: Satellite Meeting on Powder Diffraction of the XV Congress of the IUCr, 1990, p. 127.
[28] E. Zhecheva, R. Stoyanova, Solid State Ion. 66 (1993) 143.
[29] R. Kano, T. Shirane, Y. Inaba, Y. Kawamoto, J. Power Sources 68 (1997) 145.
[30] G. Prado, E. Suard, L. Fournes, C. Delmas, J. Mater. Chem. 10 (2000) 2553.
[31] E. Gaudin, F. Taulelle, R. Stoyanova, E. Zhecheva, R. Alcántara, P. Lavela, J.L. Tirado, J. Phys. Chem. B 105 (2001) 8081.
[32] G. Nuspl, M. Nagaoka, K. Yoshizawa, F. Mohri, T. Yamabe, Bull. Chem. Soc. Jpn. 71 (1998) 2259.
[33] R. Alcantara, P. Lavela, J.-L. Tirado, R. Stoyanova, E. Kuzmanova, E. Zhecheva, Chem. Mater. 9 (1997) 2145.
[34] R. Stoyanova, E. Zhecheva, C. Friebel, J. Phys. Chem. Solids 54 (1993) 9.
[35] R. Stoyanova, E. Zhecheva, C. Friebel, Solid State Ion. 73 (1994) 1.
[36] R. Stoyanova, E. Zhecheva, R. Alcantara, P. Lavela, J.-L. Tirado, Solid State Commun. 102 (1997) 457.
[37] R. Stoyanova, E. Zhecheva, R. Alcántara, J.L. Tirado, J. Phys. Chem. B 108 (2004) 4053.